Hindawi
Geofluids
Volume 2021, Article ID 8926423, 13 pages
https://doi.org/10.1155/2021/8926423

Research Article

Study on the Reinforcing Effects of the FRP-PCM Method on Tunnel Linings for Dynamic Strengthening

Xiaoshan Wang,[1] **Lin Wei**,[1] **Zaiquan Wang**,[1] **Yujing Jiang**,[2,3] **Liming Zhang**,[1] **Fanzhen Meng**,[1] **and Yu Cong**[1]

[1]*College of Science, Qingdao University of Technology, Qingdao, Shandong 266033, China*
[2]*State Key Laboratory of Mining Disaster Prevention and Control Co-Founded by Shandong Province and the Ministry of Science and Technology, Shandong University of Science and Technology, Qingdao 266590, China*
[3]*Graduate School of Engineering, Nagasaki University, Nagasaki 852-8521, Japan*

Correspondence should be addressed to Xiaoshan Wang; wangxiaoshan@qut.edu.cn

Received 7 September 2021; Accepted 25 September 2021; Published 7 October 2021

Academic Editor: Zhijie Wen

In recent years, fiber-reinforced plastic (FRP) has been widely used in the reinforcement of concrete structure fields due to its favorable properties such as high strength, low weight, easy handling and application, and immunity to corrosion, and the reinforcing effects with FRP grids on tunnel linings should be quantitatively evaluated when the tunnels encounter an earthquake. The aim of the present study is to estimate the reinforcing effects of fiber-reinforced plastic (FRP) grids embedded in Polymer Cement Mortar (PCM) shotcrete (FRP-PCM method) on tunnel linings under the dynamic load. A series of numerical simulations were performed to analyze the reinforcing effects of FRP-PCM method quantitatively, taking into account the impacts of tunnel construction method and cavity location. The results showed that the failure region on lining concrete is improved obviously when the type CII ground is encountered, regardless the influences of construction method and cavity location. With the increment of ground class from CII to DII, the axial stress reduction rate R_σ increases from 13.18% to 48.60% for tunnels constructed by the NATM, while for those tunnels constructed by the NATM, R_σ merely varies from 0.72% to 2.11%. R_σ decreases from 43.35% to 34.80% when a cavity exists on the shoulder of lining, while decreasing from 14.7% to 0.12% when a cavity exists on the crown of lining concrete. All those conclusions could provide valuable guidance for the reinforcing of underground structures.

1. Introduction

Although the dynamic mechanical behavior of underground structures, such as tunnels and underground caverns, is assumed to be better than that of surface structures, some existing tunnels still have been severely damaged by earthquakes in recent years [1–8]. Cracking, spalling, and water leakage occurring during earthquakes would significantly affect the safety of tunnel operation. The repair and reinforcement of existing underground concrete structures has become an import part of civil engineering activities.

A series of methods have been adopted to effectively improve the integrity of concrete structures in existing tunnels, the typical ones of which are grouting reinforcement method, fiber reinforced shotcrete (FRS) method [9–13], carbon fiber sheet (CFS) method [14–16], steel board method [17], and fiber-reinforced plastic (FRP) method [18, 19]. Due to the favorable properties such as high strength, low weight, easy handling and application, and immunity to corrosion, FRP as a strengthening material for the reinforcement concrete (RC) structures has become commonly used in engineering fields. In the reinforcement of mountain tunnel, the FRP grids embedded in Polymer Cement Mortar (FRP-PCM) shotcrete (FRP-PCM method) are typically used. In the FRP-PCM method, the FRP grids are firmly installed on an existing tunnel lining concrete with concrete anchors (see Figure 1(a)). It is noted that the FRP grids should not be damaged during the drilling or

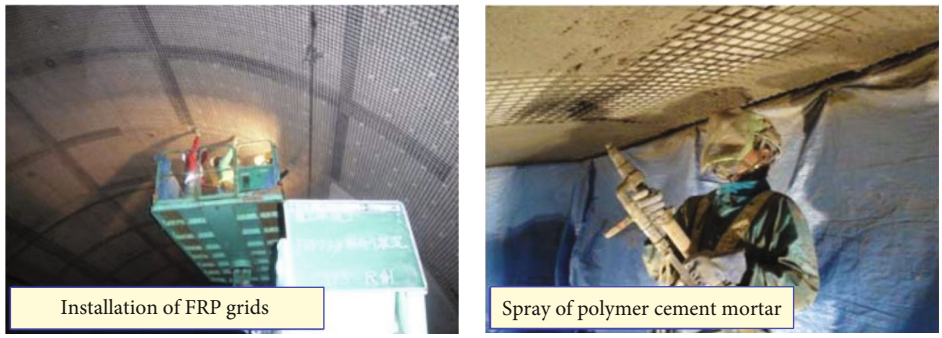

(a) Installation of FRP grids (b) Spray of Polymer Cement Mortar

Figure 1: Reinforcement procedure with the FRP-PCM method.

fastening the anchors. After the installation of FRP grids, the Polymer Cement Mortar (PCM) is sprayed to the surface of FRP grids as shown in Figure 1(b).

In recent years, extensive researches have been carried out to investigate the reinforcing effects of FRP grids under dynamic load. Sheikh and Yau [20] conducted an experimental program in which 12 column specimens were tested under constant axial load and cyclic lateral load to simulate the earthquake loads and found that the strength, ductility, and energy absorption capacity of columns can be improved by utilizing FRP. Zou et al. [21] proposed an optimization technique for the performance-based seismic FRP retrofit design of reinforced concrete (RC) building frames, and the effectiveness of this proposed procedure was discussed and certified by a numerical example. Antoniades et al. [22] conducted cyclic tests on seismically damaged reinforced concrete walls strengthened with FRP reinforcement, and the test results showed that the strength of specimen reinforced by FRP strips increases up to approximately 30% with respect to a conventional repair method. Lam et al. [23] experimentally studied the behaviors of FRP-confined concrete under cyclic compression test, and a number of significant conclusions were drawn, including the existence of an envelope curve and the cumulative effect of loading cycles. Zhou et al. [24] conducted the dynamic three-point bending and axial crushing tests to investigate the dynamic crushing characteristics of unidirectional carbon fiber-reinforced plastic composites, and the results showed that delamination plays a critical role in the dynamic bending deformation. Jerome and Ross [25] numerically simulated the dynamic response of concrete beams that reinforced with a carbon fiber plastic by using the drop-weight impact test, and the numerical results revealed the local displacement behavior of beams when suffering from strong impulse loads.

Despite a large number of researches on the behavior of RC structures reinforcing with FRP were performed, few researches were conducted on the reinforcing effects of the FRP-PCM method on tunnel lining under dynamic load. In the present study, a series of numerical simulations were performed based on the finite difference method (FDM) to quantitatively analyze the reinforcing effects of the FRP-PCM method under dynamic load, taking into account the impacts of tunnel construction method and cavity location, and those analytic results could provide valuable guidance for the reinforcing of underground structures.

2. Numerical Modelling Setup

2.1. Numerical Modelling. The New Austrian Tunneling Method (NATM) and the Fore-piling Method (FM) are the two common methods that have been adopted in tunnelling under shallow or unconsolidated ground (Kitamoto et al., 2004). In the present study, four types of numerical models as shown in Figure 2 are established by utilizing the finite difference method (FDM), and the former two models (see Figures 2(a) and 2(b)) are selected to investigate the effects of construction methods on reinforcing effects of the FRP-PCM method. Since cavities that exist between tunnel lining and surrounding rocks are generally encountered for mountain tunnels constructing with the FM method, a cavity is presumed to exist on the crown (see Figure 2(c)) or at the shoulder (see Figure 2(d)) of the numerical models to investigate the impacts of cavity location on the reinforcing effects. Those cavities cover an angle of 60° and with a thickness of 30 cm. The thickness of shotcrete and secondary lining in the NATM method are set to be 15 cm and 30 cm, respectively, and the lining thickness in the FM method is selected as 45 cm. The reinforcement region with the FRP-PCM method covers an arc length of 180° on the upper wall of tunnel as shown in Figure 3, and the back-filling is conducted to the tunnels with cavities. The tunnel linings are reproduced by the finite element mesh, while the reinforcing effects of the FRP-PCM method are investigated by the liner element [26].

2.2. Boundary Conditions. In order to reduce the computational time and ensure the calculation accuracy, the horizontal distance from the wall of tunnel to the boundary of the main grid model is determined as $2D$ (D is the excavation width of tunnel that is equal to 10 m) based on the precomputation. The dynamic load input is applied at the bottom of the model and normally represented by plane waves propagating upward through the underlying rocks. The free-field boundary conditions are selected during the seismic analysis to minimize the wave reflections, and the lateral boundaries of the main grid are coupled to the free-field grid boundary by a series of viscous dashpots as shown in Figure 4 [26]. By

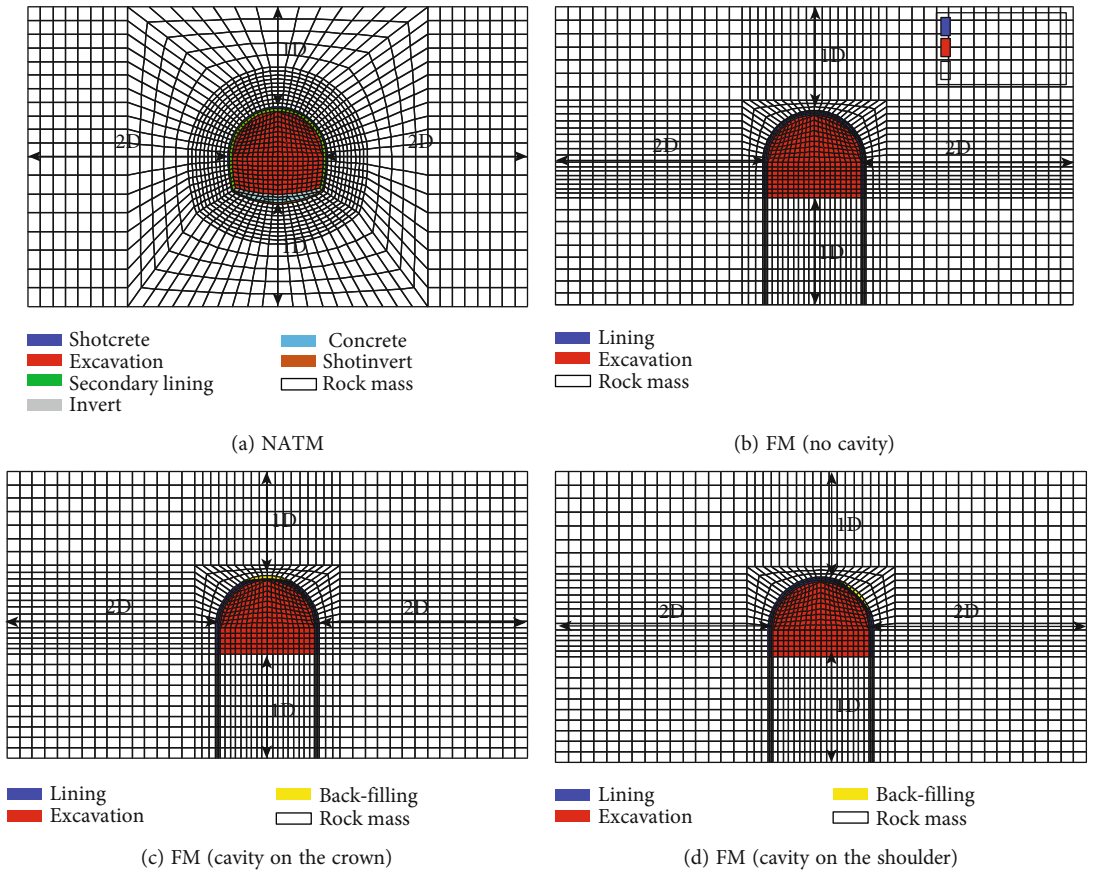

Figure 2: Numerical modelling setup.

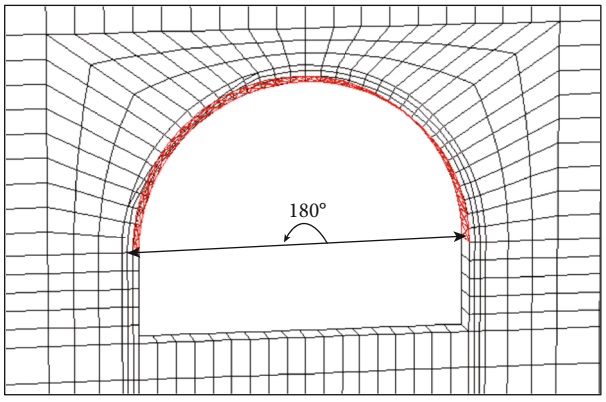

Figure 3: Reinforcing region with the FRP-PCM method.

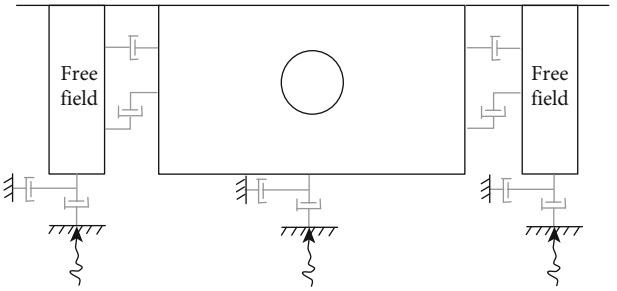

Figure 4: Free-field boundary for dynamic analysis.

means of which, plane waves propagating upward surf no distortion at the boundary because the free field grid supplies conditions that are identical to those in an infinite model. Lateral dashpots would not do exercise if the main grid in uniform with no surface structure, since the free field grid performs the same as the main grid, while the dashpots absorb energy in a manner to quiet boundaries if the main grid motion differs from that of the free filed.

2.3. Mechanical Properties. Three types of ground classed as CII, DI, and DII generally encountered in mountain tunnel construction in Japan [27] are selected as the surrounding rocks in the numerical analysis, and the mechanical behaviors of those are listed in Table 1. The urethane material is utilized as the back-filling material due to its quick harden and high strength, and the mechanical properties of back-filling material and lining concrete are also summarized in Table 1. The mechanical behaviors of the interface between the FRP-PCM layer and the concrete layer are obtained based on a series of direct shear tests in our previous study [28], and those values are summarized in Table 2.

2.4. Input Motion. Compared with artificial seismic waves and simple harmonic waves, real seismic wave taken from similar sites is more representative to the real situation when

Table 1: Mechanical behaviors of ground, lining, and back-filling material.

Properties	Ground class				Lining	Back-filling material
	CI	CII	DI	DII		
γ (kN/m^3)	23.5	22.6	21.6	20.6	24	9.8
E (MPa)	1960	980	490	147	24500	12
ν	0.3	0.3	0.35	0.35	0.2	0.13
c (MPa)	1.96	0.98	0.49	0.196	6.99	0.5
φ (deg)	45	40	35	30	40	10
σ_t (MPa)	0.39	0.42	0.19	0.06	3	0.2

Table 2: Mechanical properties of FRP grids and PCM material.

		Elastic modulus (MPa)	Compressive strength (MPa)	Tensile strength (MPa)	Cohesion (MPa)	Internal friction angle (°)	Cross-sectional area of mesh (mm^2)
FRP grid	CR4	1×10^5	—	1400	2.22	17.7	6.6
	CR6						17.5
	CR8						26.4
PCM		2.6×10^4	59.3	4.6			—

a rock foundation is subjected to earthquake loads. In the present study, the input motion is recorded at the observation site of Ojiya City during the M6.8 Chuetsu offshore earthquake happened on July 16, 2007, in Niigata Prefecture, Japan. The distributions of intensities and peak accelerations during the earthquake are shown in Figure 5. Since rock foundations and buildings are easier to damage when they suffer from shear waves, compared with a compression one, the horizontal component motion of ground (see Figure 6) is adopted in the later numerical analysis. The maximum acceleration is observed at about 27.8 s, with a value about 330 Gal. Since the stability of underground tunnel is mainly controlled by the maximum acceleration during the earthquake, in order to reduce the computational time, the input motion at the interval from 20.8 s to 30.8 s is extracted and utilized in the latter numerical analysis.

3. Numerical Results

3.1. Reinforcing Effects for Tunnels Constructed with the NATM. Figure 7 shows the distribution of plastic failure region on lining concrete for tunnels constructed by the NATM. For the unreinforced cases, the plastic failure region first appears at the bottom corner and inner side of the shoulder on lining concrete and gradually expands with the increment of ground class (see Figures 7(a)–(c)). For the type DII ground, the plastic failure region develops at both the inner side and the outer side of lining concrete. After reinforcing with FRP grids, the plastic failure zone on the shoulder diminishes and only can be observed at the bottom corner when the type CII ground is encountered (Figure 7(d)). The plastic failure region at the inner side of the left shoulder decreases greatly when the tunnels surround by the type DI ground (Figure 7(e)).

Tunnel lining deformations are generally governed by both the axial stress parallel to the tunnel wall and the radial stress perpendicular to the tunnel wall. Since the axial stress is approximately two orders of magnitude larger than the radial one, only the variation of axial stress is analyzed in the present study to illustrate the reinforcing effects with the FRP-PCM method. The axial stress distribution on lining concrete for tunnels constructed by the NATM is shown in Figure 8. In those figures, the positive symbol denotes the compression stress, while the negative symbol denotes the tensile stress. Since the input motion is a horizontal shear signal, the maximum tension and compression stresses occur at the left and right shoulder of tunnel lining, respectively. The maximum tension stress can also be observed at the bottom corner of lining concrete due to stress concentration. The maximum tension stresses at the bottom corner or shoulder of lining concrete are 2.77 MPa, 4.73 MPa, and 9.56 MPa, respectively, corresponding to the ground type of CII, DI, and DII (Figures 8(a)–8(c)). After reinforcing with FRP grids, those maximum tension stresses decrease to 2.75 MPa, 4.63 MPa, and 9.53 MPa, respectively (Figures 8(d)–8(f)).

3.2. Reinforcing Effects for Tunnels Constructed with the FM. Figure 9 shows the distribution of plastic failure region on lining concrete for tunnels constructed by the FM. The plastic failure region can be observed at the right inner side of lining concrete as shown in Figure 9(a) for the type CII ground. With the increment of ground class, the strength of surrounding rock reduces, and the plastic failure regions both occur at the left outer side and right inner side of lining concrete (Figures 9(b) and 9(c)). After reinforcing with FRP grids, almost no plastic failure region is observed when the CII ground is encountered (Figure 9(d)), and the plastic failure region decreases obviously when the other two types of ground are encountered (Figures 9(e) and 9(f)).

The axial stress distribution on lining concrete for tunnels constructed by the FM is depicted in Figure 10. Under a horizontal shear load, the maximum tension

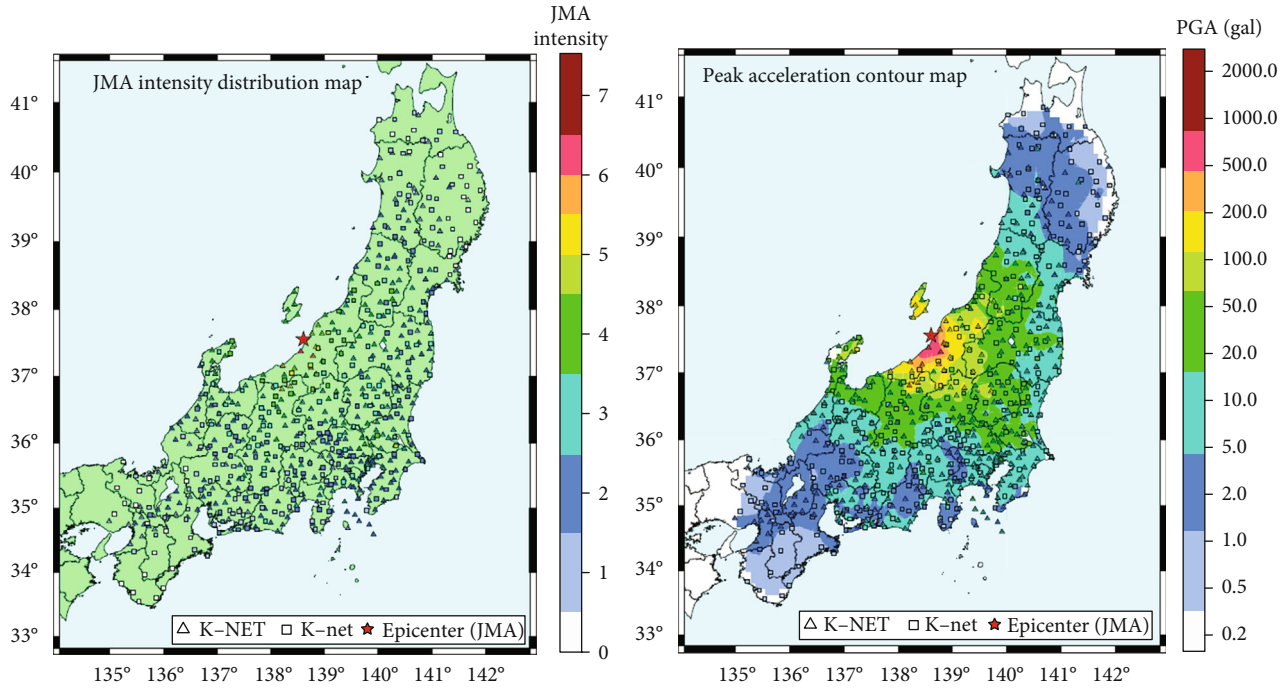

(a) Distribution of intensities

(b) Distribution of peak accelerations

Figure 5: Distributions of intensities and peak accelerations recorded at the observation site of Ojiya City during the M6.8 Chuetsu offshore earthquake happened on July 16, 2007, in Niigata Prefecture, Japan.

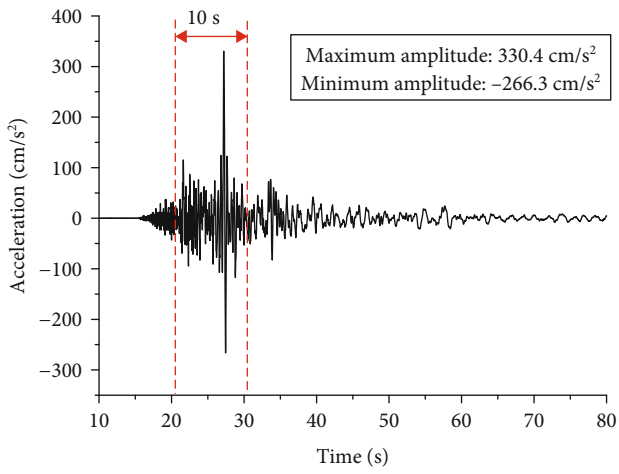

Figure 6: Input motion adopted in the numerical simulations.

and compression stress appear at both sides of the lining shoulder. The maximum tension stress mainly occurs at the left inner side of lining concrete, and the maximum compression one almost can be observed at the right inner of lining concrete. The maximum compression stresses are 2.2 MPa, 8.28 MPa, and 14.16 MPa (Figures 10(a)–10(c)), respectively, corresponding to the type CII, DI, and DII ground. After reinforcing with FRP grid, those compress values decrease to 1.91 MPa, 4.81 MPa, and 7.42 MPa, respectively (Figures 10(d)–10(f)).

3.3. Reinforcing Effects for Tunnels with a Cavity on the Shoulder. The plastic failure region on lining concrete for tunnels with a cavity on the shoulder is shown in Figure 11. Due to the existence of cavity on the shoulder, the flexural rigidity of lining concrete decreases, leading to a larger plastic failure region that appears at the location of cavity. As what mentioned before, the plastic failure region can also be generated at the shoulder of lining concrete due to the application of horizontal shear load. After reinforcing with FRP grids, the plastic failure region on the lining concrete disappears for the type CII ground (Figure 11(d)), and those plastic failure regions decrease dramatically for the other two types of ground (Figures 11(e) and 11(f)).

The axial stress on lining concrete for tunnels with a cavity on the shoulder is plotted in Figure 12. The existence of cavity on the shoulder decreases the bending resistance of lining concrete, and the stress concentration is easy to occur at the thin lining concrete, leading to a great value of axial stress at those locations. The maximum values at the cavity for those three types of ground are 4.90 MPa, 8.10 MPa, and 10.06 MPa (Figures 12(a)–12(c)), respectively, and those values decrease to 2.77 MPa, 4.33 MPa, and 6.56 MPa after reinforcing with FRP grids (Figures 12(d)–12(f)).

3.4. Reinforcing Effects for Tunnels with a Cavity on the Crown. The plastic failure region for tunnels with a cavity on the crown is first observed at the top right shoulder of the lining concrete (Figure 13(a)). With increasing the ground class, the plastic failure region develops and mainly

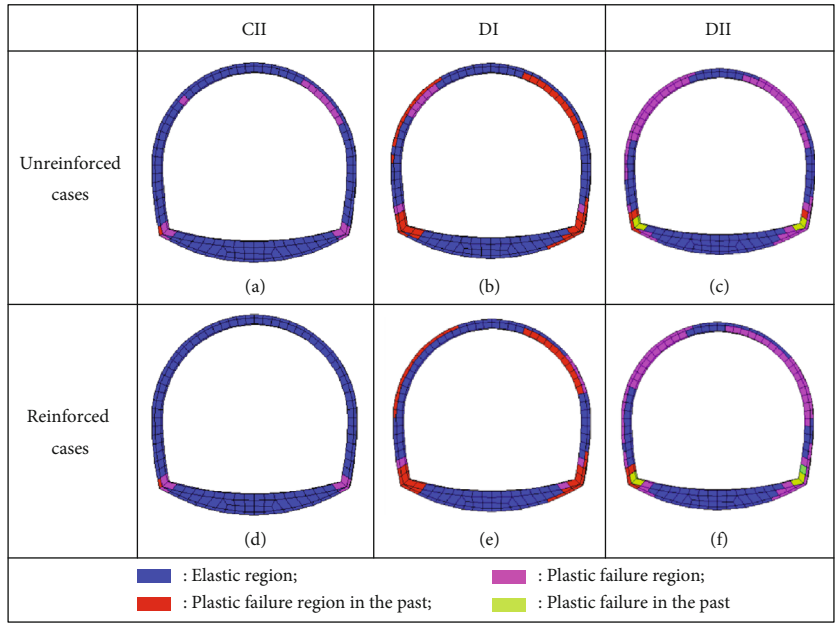

Figure 7: Plastic failure region on lining concrete for tunnel constructed by NATM.

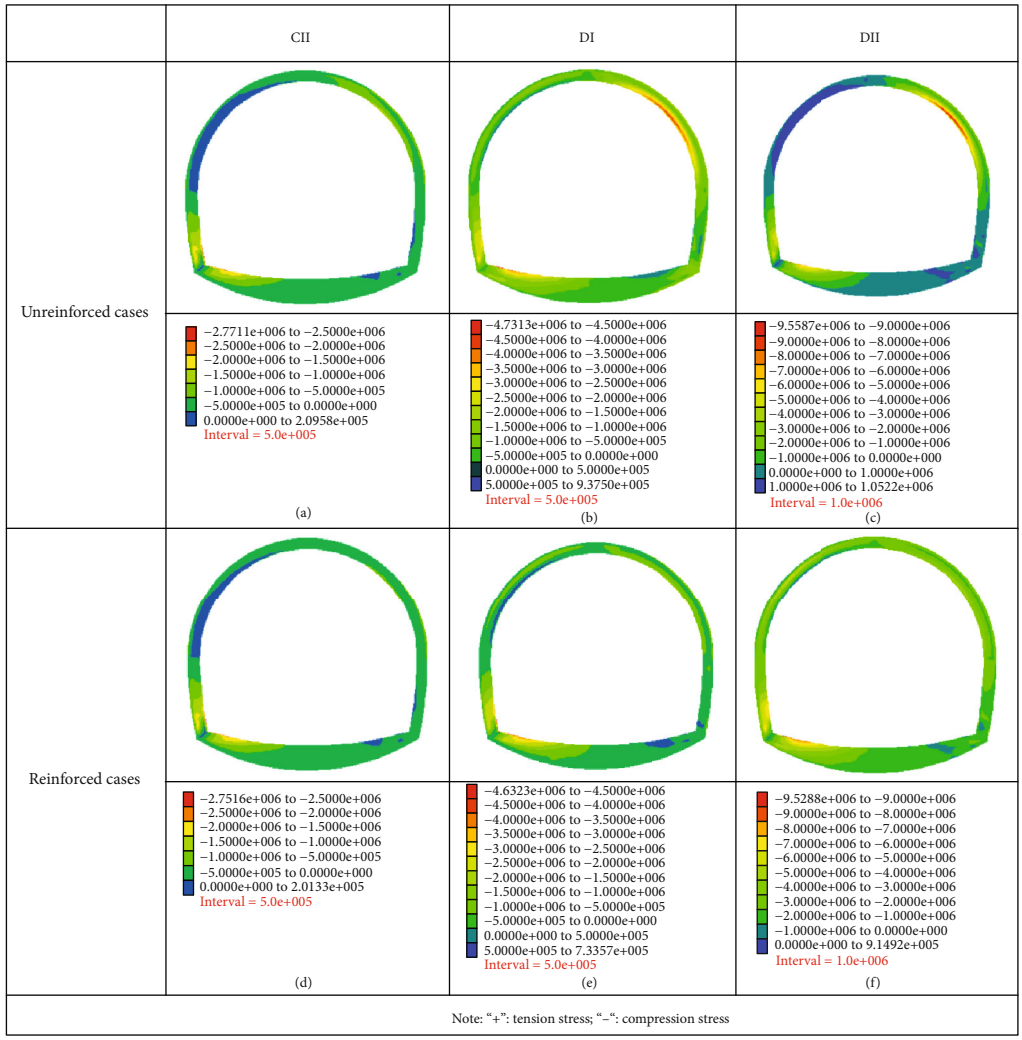

Figure 8: Axial stress distribution on lining concrete for tunnel constructed by NATM (unit: Pa).

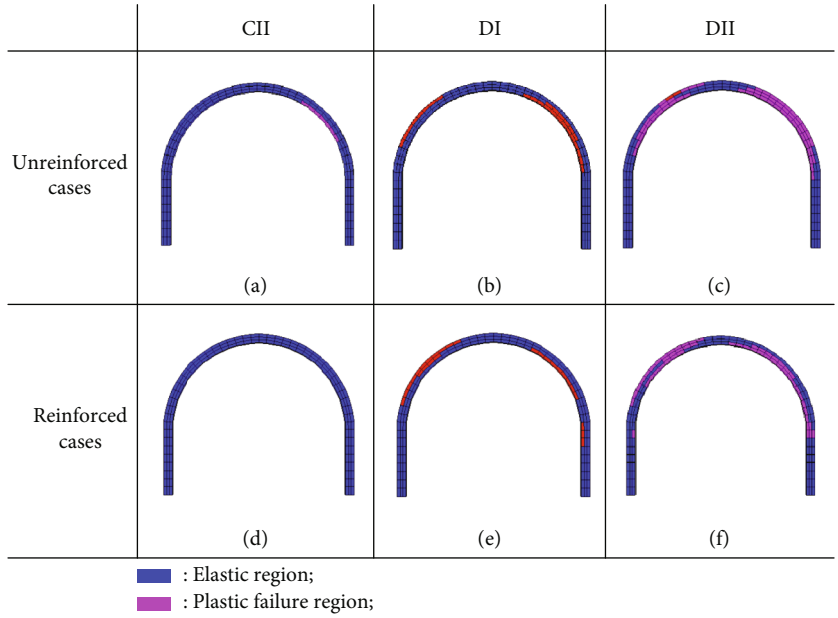

Figure 9: Plastic failure region on lining concrete for tunnel constructed by FM.

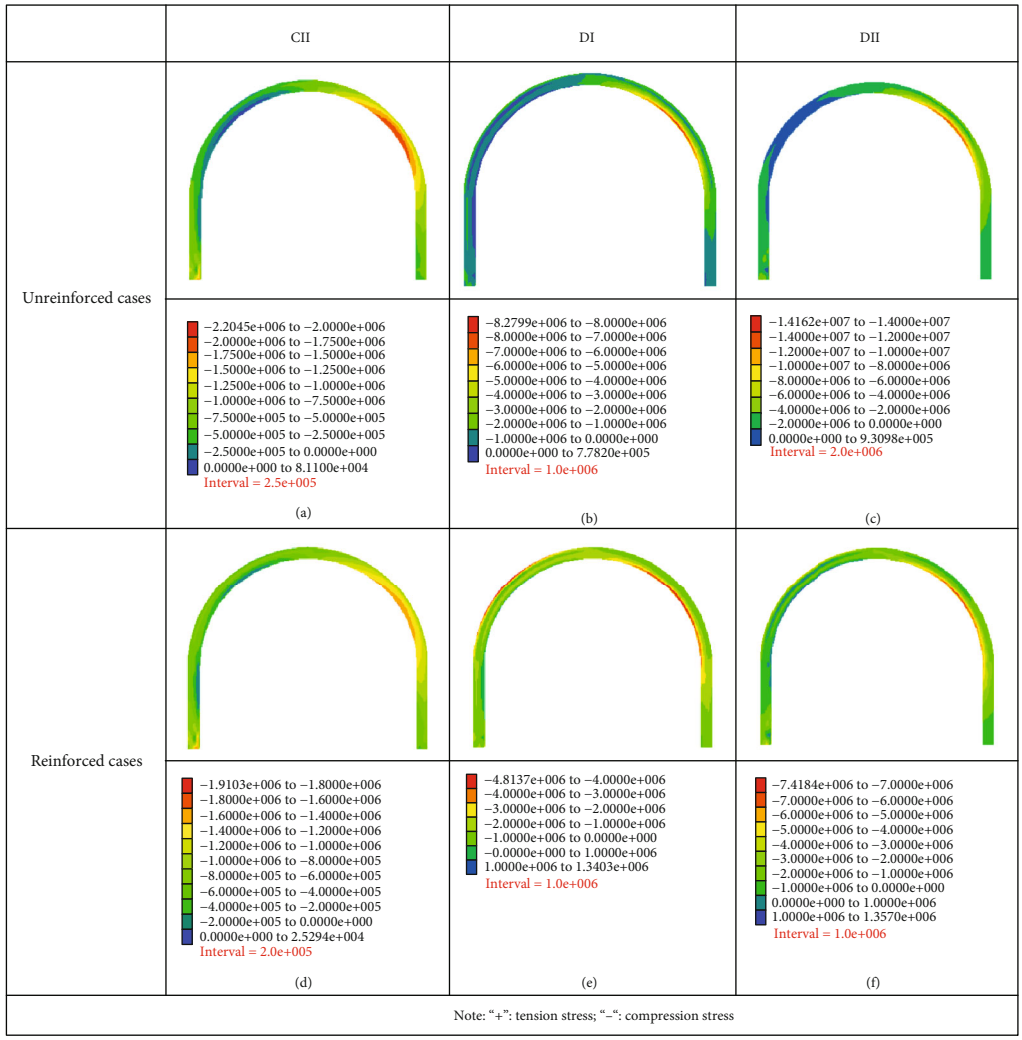

Figure 10: Axial stress distribution on lining concrete for tunnel constructed by FM (unit: Pa).

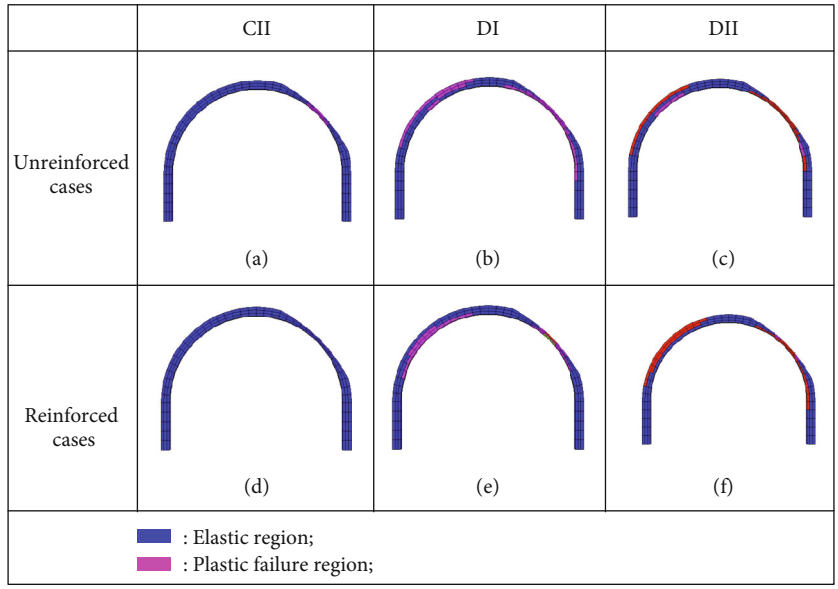

Figure 11: Plastic failure region on lining concrete for tunnel with a cavity on the shoulder.

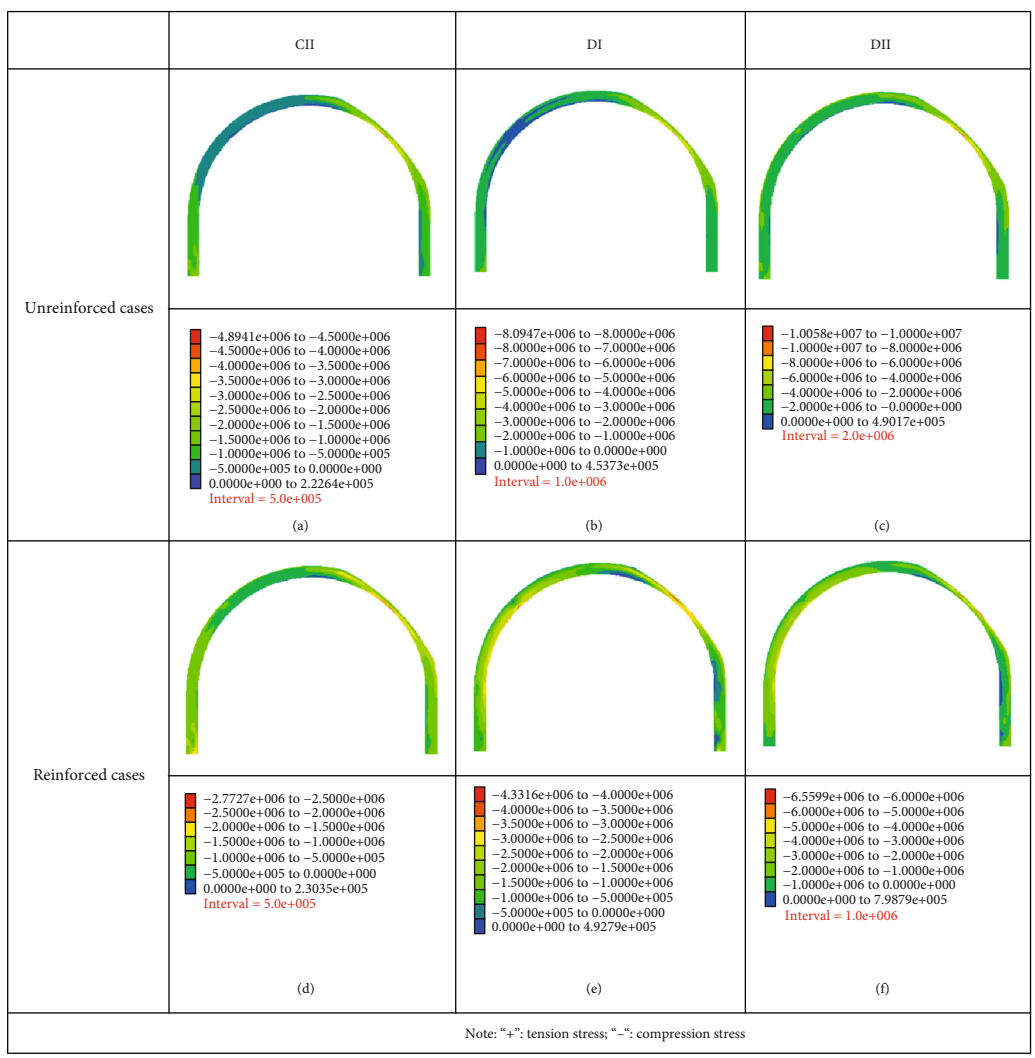

Figure 12: Axial stress distribution on lining concrete for tunnel with a cavity on the shoulder (unit: Pa).

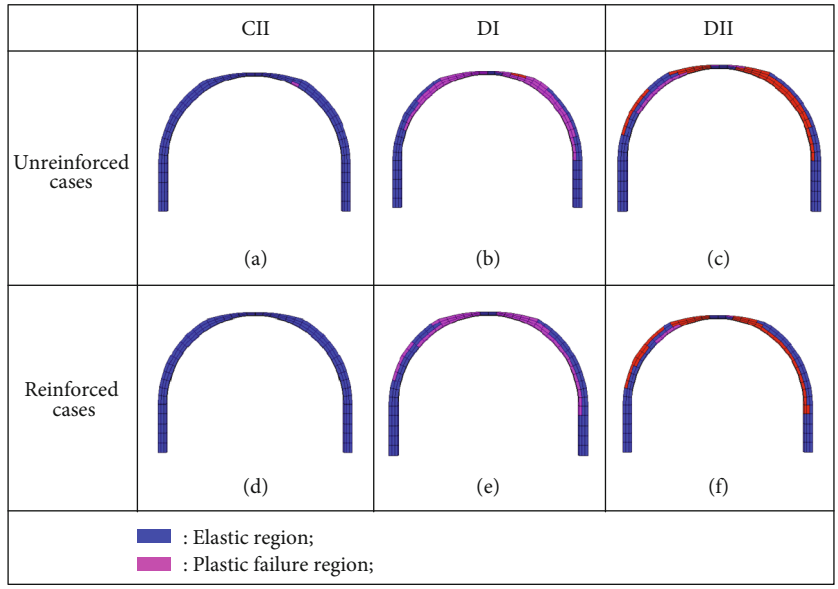

Figure 13: Plastic failure region on lining concrete for tunnel with a cavity on the crown.

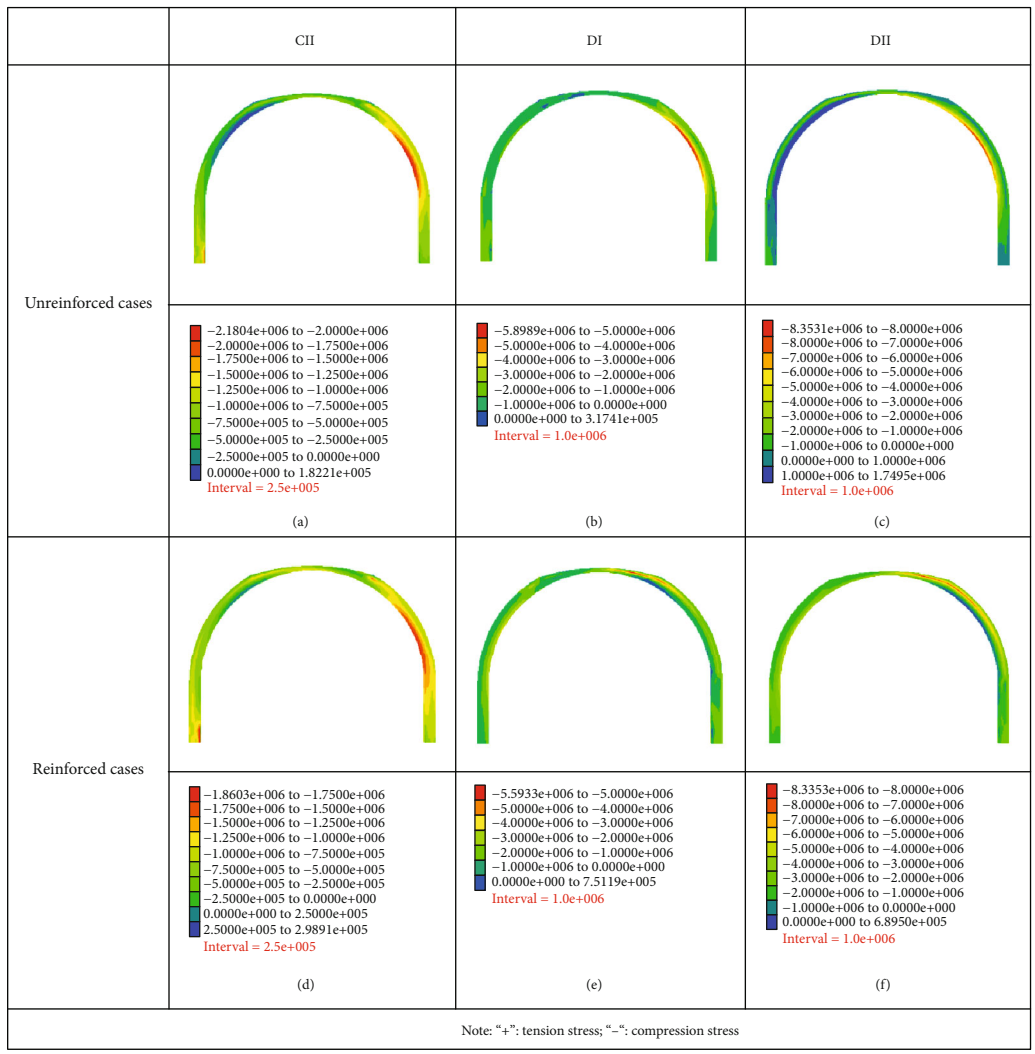

Figure 14: Axial stress distribution on lining concrete for tunnel with a cavity on the crown (unit: Pa).

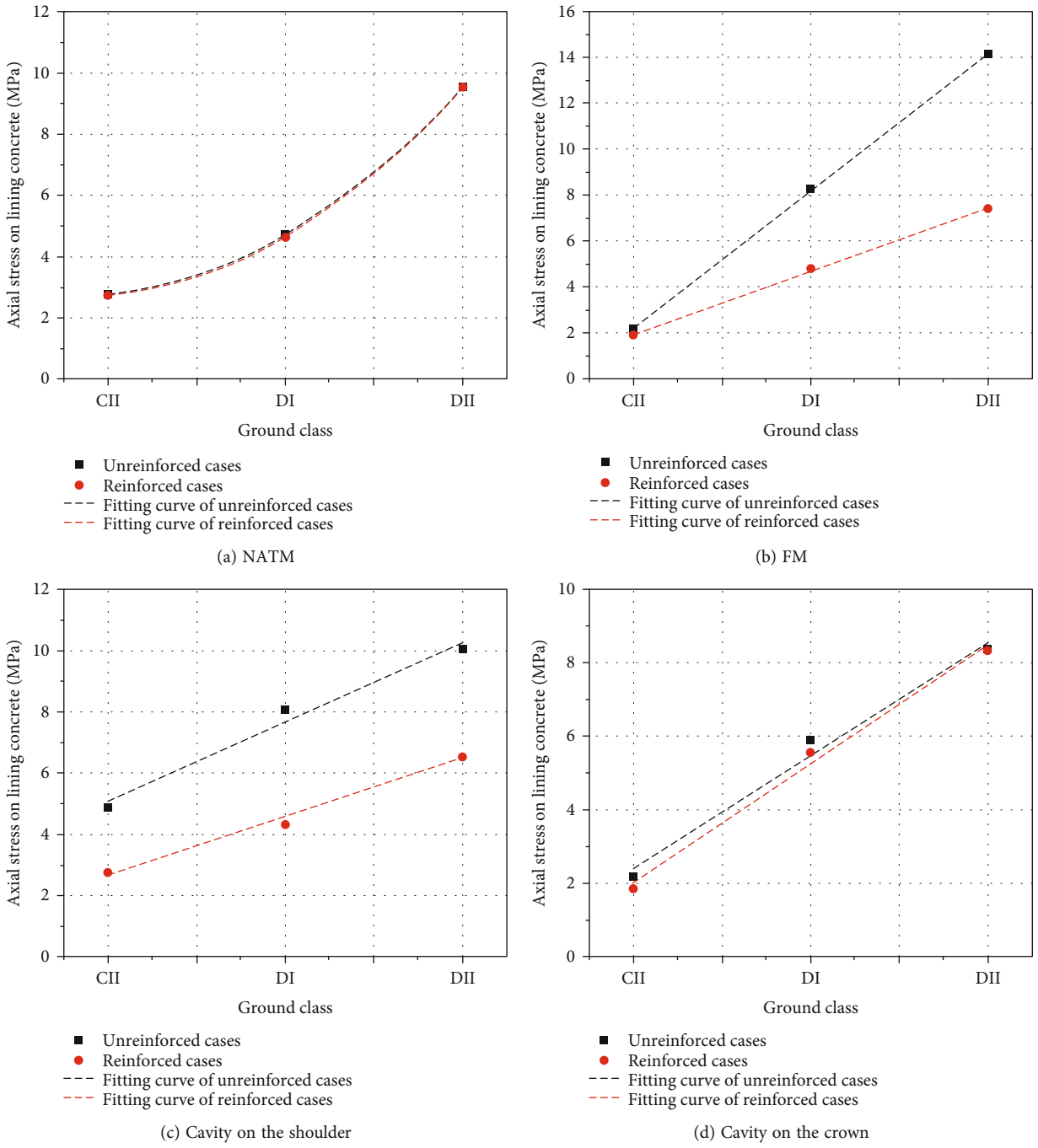

Figure 15: The variation of maximum axial stress on lining concrete.

concentrates at the right inner and left inner sides of lining concrete. The failure region vanishes after reinforcing with FRP grids for the type CII ground (Figure 13(d)) and does not dramatically decrease for the other two types of ground (Figures 13(e) and 13(f)).

The axial stress distribution on the lining concrete for tunnels with a cavity on the crown is shown in Figure 14. The maximum values of compression stress on the right shoulder of lining are 2.08 MPa, 5.89 MPa, and 8.35 MPa, respectively, corresponding to the three types of ground (Figures 9(a)–9(c)). And those values decrease to 1.86 MPa, 5.59 MPa, and 8.34 MPa, respectively (Figures 9(d)–9(f)).

4. Discussion

Figure 15 shows the relationship between the ground class and the maximum axial stress on a lining concrete for the reinforced and unreinforced cases. The maximum axial stress on lining concrete increases with ground class, regardless of the tunnel construction method, existence of cavity,

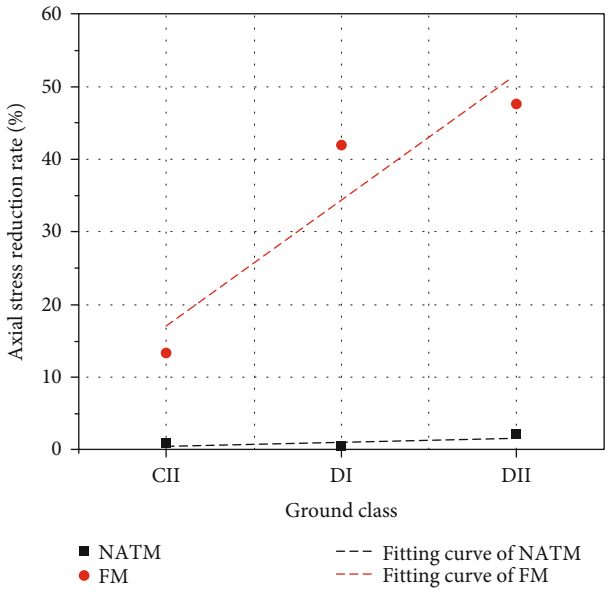

Figure 16: The axial stress reduction rate on lining concrete for tunnels constructed by different methods.

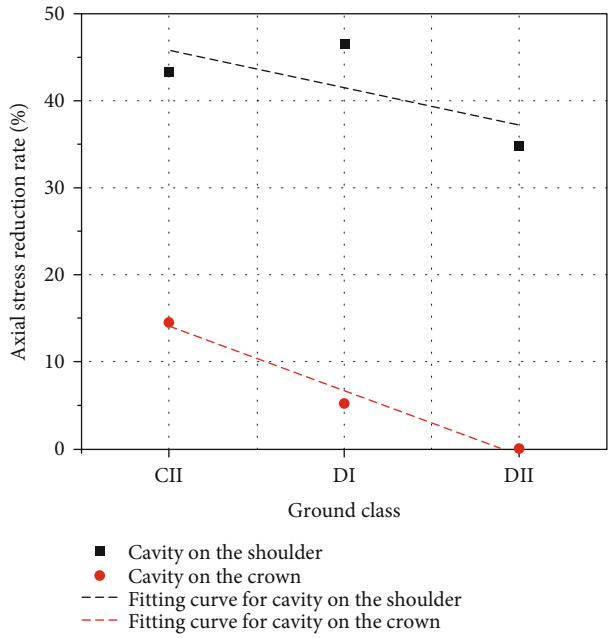

Figure 17: The axial stress reduction rate on lining concrete for tunnels with a cavity.

and reinforcing with FRP grids. However, for tunnels constructed by the NATM, the fitting curves of axial stress for the reinforced one and unreinforced one almost increase nonlinearly, indicating that with decreasing in rock strength, the axial stress on lining concrete increases dramatically (Figure 15(a)). The two fitting curves also show that the axial stress rarely decreases after reinforcing with FRP grids for tunnel constructed by the NATM. The fitting lines of axial stress for tunnel constructed by the FM increase linearly as shown in Figure 15(b). The fitting curves for the reinforced cases and unreinforced cases intersect at the ground class of CII, indicating that the reinforcing effects are not obvious when type CII ground is encountered. With the increment of ground class, stress reduction shows more significant after reinforcing with FRP grids, indicating that better reinforcing effects could be obtained when a weaker surrounding rock is encountered. Although the axial stress on a lining concrete increases with increasing the ground class when a cavity exists on the shoulder of tunnel lining, the slope of fitting curve shows slightly decrement, indicating that the reinforcing effects with FRP grids increase with the increment in ground class (Figure 15(c)). While for those tunnels with a cavity on the crown, the fitting curves almost intersect at the point of the largest ground class (i.e., class DII ground) as shown in Figure 15(d), which demonstrated that the reinforcing effects of the FRP-PCM method are not obvious for a higher class of ground.

In order to investigate the reinforcing effects of the FRP-PCM method quantitatively, an axial reduction rate R_σ defined as follows is calculated:

$$R_\sigma = \frac{\sigma_{nr} - \sigma_r}{\sigma_{nr}} \times 100\%, \quad (1)$$

where σ_{nr} is the axial acting on the unreinforced lining (MPa) and σ_r is the axial stress obtained in the reinforced cases (MPa). Since the axial stress is the principle stress parallel to the tunnel lining, the axial force reduction rate represents the degree of reduction in axial stress after reinforcing with FRP grids.

Figure 16 shows the relationship between axial stress reduction rate and ground class, taking into account the construction method. R_σ increases with the increasing ground class for tunnels constructed by the FM, revealing that the performance of reinforcement is greater when a higher type of ground is encountered. With the increment of ground class from CII to DII, R_σ increases from 13.18% to 48.60%. While for those tunnels constructed by the NATM, R_σ merely varies from 0.72% to 2.11%, which demonstrated that the performance of reinforcement is not obvious.

Figure 17 shows the relationship between the axial stress reduction rate and ground class, taking into account the existence of cavity. R_σ decreases with increasing in ground class, indicating that the performance of reinforcement is weaker when a higher type of ground is encountered. With the increase in ground class from CII to DII, R_σ decreases from 43.35% to 34.80% when a cavity exists on the shoulder of lining, while decreasing from 14.7% to 0.12% when a cavity exists on the crown of lining concrete. The results also demonstrate that the performance of reinforcement is greater when a cavity exists on the shoulder.

5. Conclusions

In the present study, the reinforcing effects of the FRP-PCM method under dynamic load have been investigated based on the numerical analysis, taking into account the

tunnel construction method and location of tunnel cavity. In advancing this work, the following conclusions are drawn:

(1) The plastic failure region on lining concrete is improved obviously when the type CII ground is encountered, regardless of the influences of construction methods and cavity locations

(2) For tunnels constructed by the NATM, the axial stress on lining concrete increases dramatically with the increment of ground class, and this axial stress merely changes after reinforcing with FRP grids. While for those tunnels constructed by the FM, the reinforcing effects improve with the increment of ground class

(3) The axial stress on the lining concrete merely varies after reinforcing with FRP grids for tunnels with a cavity on the crown, and a good reinforcing performance is observed for the cases with a cavity on the shoulder, compared with the one with a cavity on the crown

(4) Only the CR8 grids were taken into account during the numerical simulations under seismic load. In the future, various types of FRP grids, such as CR4 and CR6, should be discussed to investigate the reinforcing effects of the FRP-PCM method

(5) With the increment of ground class from CII to DII, R_σ increases from 13.18% to 48.60% for tunnels constructed by the NATM, while for those tunnels constructed by the NATM, R_σ merely varies from 0.72% to 2.11%. R_σ decreases from 43.35% to 34.80% when a cavity exists on the shoulder of lining, while decreasing from 14.7% to 0.12% when a cavity exists on the crown of lining concrete

Data Availability

The original data can be applied if needed.

Conflicts of Interest

The authors declare that there are no conflicts of interest regarding the publication of this article.

Acknowledgments

We gratefully acknowledge the financial support from the National Natural Science Foundation of China under Grant Nos. 51879135, 51808306, and 52179104. This work is also supported by Taishan Scholars Program (2019KJG002 and 2019RKB01083), the Natural Science Foundation of Shandong Province (ZR2019BEE051, ZR2020ME099, and ZR2020MD111), the Foundation of the Key Laboratory of Mining Disaster Prevention and Control (MDPC202010).

References

[1] V. A. Kontogianni and S. C. Stiros, "Earthquakes and seismic faulting: effects on tunnels," *Turkish Journal of Earth Sciences*, vol. 12, no. 1, pp. 153–156, 2003.

[2] T. D. O'Rourke, S. H. Goh, C. O. Menkiti, and R. J. Mair, "Highway tunnel performance during the 1999 Duzce earthquake," in *XV International Conference on Soil Mechanics and Geotechnical Engineering*, Istanbul Turkey, August 2001.

[3] Y. Shen, B. Gao, X. Yang, and S. Tao, "Seismic damage mechanism and dynamic deformation characteristic analysis of mountain tunnel after Wenchuan earthquake," *Engineering Geology*, vol. 180, pp. 85–98, 2014.

[4] T. Suzuki, "Damages of urban tunnels due to the Southern Hyogo earthquake of January 17, 1995 and the evaluation of seismic isolation effect," in *CD-ROM of the 11WCEE*, Elsevier, Acapulco, Mexico, 1996.

[5] X. Zhang, Y. Jiang, and S. Sugimoto, "Seismic damage assessment of mountain tunnel: a case study on the Tawarayama tunnel due to the 2016 Kumamoto earthquake," *Tunnelling and underground space technology*, vol. 71, pp. 138–148, 2018.

[6] J. N. Wang and G. A. Munfakh, "Seismic design of tunnels," *WIT Transactions on the Built Environment*, vol. 57, 2001.

[7] N. Yoshida, "Ungerground and buried structure, earthquake geotechnical engineering," in *Proceedings of 2nd International Conference on Earthquake Geotechnical Engineering*, Chengdu, China, 1999.

[8] H. Yu, J. Chen, A. Bobet, and Y. Yuan, "Damage observation and assessment of the Longxi tunnel during the Wenchuan earthquake," *Tunnelling and Underground Space Technology*, vol. 54, pp. 102–116, 2016.

[9] B. Chiaia, A. P. Fantilli, and P. Vallini, "Combining fiber-reinforced concrete with traditional reinforcement in tunnel linings," *Engineering Structures*, vol. 31, no. 7, pp. 1600–1606, 2009.

[10] A. De la Fuente, P. Pujadas, A. Blanco, and A. Aguado, "Experiences in Barcelona with the use of fibres in segmental linings," *Tunnelling and Underground Space Technology*, vol. 27, no. 1, pp. 60–71, 2012.

[11] V. Moreira de Alencar Monteiro and F. de Andrade Silva, "The use of the Barcelona test as quality control of fiber reinforced shotcrete for underground mining," *Construction and building materials*, vol. 262, p. 120719, 2020.

[12] T. Franzén, "Shotcrete for underground support: a state-of-the-art report with focus on steel-fibre reinforcement," *Tunnelling and Underground Space Technology*, vol. 7, no. 4, pp. 383–391, 1992.

[13] F. Jeng, M. L. Lin, and S. C. Yuan, "Performance of toughness indices for steel fiber reinforced shotcrete," *Tunnelling and Underground Space Technology*, vol. 17, no. 1, pp. 69–82, 2002.

[14] J. K. Lee and J. H. Lee, "Nondestructive evaluation on damage of carbon fiber sheet reinforced concrete," *Composite Structures*, vol. 58, no. 1, pp. 139–147, 2002.

[15] K. Miyauchi, *Estimation of strengthening effects with carbon fiber sheet for concrete column*, Japan Concrete Institute, 1997.

[16] C. Nony-Davadie, L. Peltier, Y. Chemisky, B. Surowiec, and F. Meraghni, "Mechanical characterization of anisotropy on a carbon fiber sheet molding compound composite under quasi-static and fatigue loading," *Journal of Composite Materials*, vol. 53, no. 11, pp. 1437–1457, 2019.

[17] K. Kiriyama, M. Kakizaki, T. Takabayashi, and N. Hirosawa, "Structure and construction examples of tunnel reinforcement method using thin steel panels," *Nippon Steel Technical Report*, vol. 92, pp. 45–50, 2005.

[18] M. A. Erki and S. H. Rizkalla, "FRP reinforcement for concrete structures," *Concrete International Detroit*, vol. 15, pp. 48–52, 1993.

[19] D. A. Hensher, *Fiber-Reinforced-Plastic (FRP) Reinforcement for Concrete Structures: Properties and Applications*, Elsevier Science, 2013.

[20] S. A. Sheikh and G. Yau, "Seismic behavior of concrete columns confined with steel and fiber-reinforced polymers," *ACI Structural Journal*, vol. 99, no. 1, pp. 72–80, 2002.

[21] X. K. Zou, J. G. Teng, L. De Lorenzis, and S. H. Xia, "Optimal performance-based design of FRP jackets for seismic retrofit of reinforced concrete frames," *Composites Part B: Engineering*, vol. 38, no. 5-6, pp. 584–597, 2007.

[22] K. K. Antoniades, T. N. Salonikios, and A. J. Kappos, "Cyclic tests on seismically damaged reinforced concrete walls strengthened using fiber-reinforced polymer reinforcement," *Structural Journal*, vol. 100, no. 4, pp. 510–518, 2003.

[23] L. Lam, J. G. Teng, C. H. Cheung, and Y. XIAO, "FRP-confined concrete under axial cyclic compression," *Cement and Concrete Composites*, vol. 28, no. 10, pp. 949–958, 2006.

[24] G. Zhou, Q. Sun, J. Fenner et al., "Crushing behaviors of unidirectional carbon fiber reinforced plastic composites under dynamic bending and axial crushing loading," *International Journal of Impact Engineering*, vol. 140, 2020.

[25] D. M. Jerome and C. A. Ross, "Simulation of the dynamic response of concrete beams externally reinforced with carbon-fiber reinforced plastic," *Computers & Structures*, vol. 64, no. 5-6, pp. 1129–1153, 1997.

[26] Itasca Consulting Group, Inc, *FLAC3D User's Manual*, 2002.

[27] The Ministry of Public Works Research Institute Tunnel Laboratory, *Document: Prediction and Measures Manuals of Ground Deformation for Tunnel Excavation (Plan)*, 1994.

[28] Y. Jiang, X. Wang, B. Li, Y. Higashi, K. Taniguchi, and K. Ishida, "Estimation of reinforcing effects of FRP-PCM method on degraded tunnel linings," *Soils and Foundations*, vol. 57, no. 3, pp. 327–340, 2017.